# **INTERFACE**

royalsocietypublishing.org/journal/rsif

# Research



**Cite this article:** Samsami K, Sanchez Arias L, Redd H, Stoll R, Pepper RE, Fu HC. 2024 Incorporating recirculation effects into metrics of feeding performance for current-feeding zooplankton. *J. R. Soc. Interface* **21**: 20230706. https://doi.org/10.1098/rsif.2023.0706

Received: 29 November 2023 Accepted: 5 February 2024

#### **Subject Category:**

Life Sciences—Physics interface

#### **Subject Areas:**

biophysics, biomechanics

#### **Keywords:**

zooplankton, *Vorticella*, feeding current, filter feeding, flow visualization

#### Author for correspondence:

Henry Chien Fu

e-mail: henry.fu@utah.edu

Electronic supplementary material is available online at https://doi.org/10.6084/m9.figshare. c.7090068.

# THE ROYAL SOCIETY

# Incorporating recirculation effects into metrics of feeding performance for current-feeding zooplankton

Kiarash Samsami<sup>1</sup>, Ludivine Sanchez Arias<sup>1</sup>, Haven Redd<sup>1</sup>, Rob Stoll<sup>1</sup>, Rachel E. Pepper<sup>2</sup> and Henry Chien Fu<sup>1</sup>

(i) REP, 0000-0001-6804-8965; HCF, 0000-0002-3543-7128

The feeding performance of zooplankton influences their evolution and can explain their behaviour. A commonly used metric for feeding performance is the volume of fluid that flows through a filtering surface and is scanned for food. Here, we show that such a metric may give incorrect results for organisms that produce recirculatory flows, so that fluid flowing through the filter may have been already filtered of food. In a numerical model, we construct a feeding metric that correctly accounts for recirculation in a sessile model organism inspired by our experimental observations of Vorticella and its flow field. Our metric tracks the history of current-borne particles to determine if they have already been filtered by the filtering surface. Examining the pathlines of food particles reveals that the capture of fresh particles preferentially involves the tips of cilia, which we corroborate in observations of feeding Vorticella. We compare the amount of fresh nutrient particles carried to the organism with other metrics of feeding, and show that metrics that do not take into account the history of particles cannot correctly compute the volume of freshly scanned fluid.

#### 1. Introduction

Zooplankton are a subgroup of planktonic organisms that cannot generate their own food and have to gather it from their environment. They comprise an important part of the food cycle in the oceans by linking the autotrophic plankton to larger animals. Since feeding performance affects survival advantages, it may explain the evolution of certain physiological traits or behaviours [1]. To understand how physiological traits affect feeding, we need a quantitative measure of feeding performance. Such a feeding performance metric should depend solely upon an organism's geometry and the gait of its moving parts. Zooplankton can be put in different categories based on how they feed, including ambush feeding, current feeding and cruise feeding [2]. In this work, we focus on current feeding, more specifically filter feeding, in which the organism generates flows through periodic motions and uses the flows to bring nutrient particles to a filtering surface and capture them. Over many periods, the fluid is continuously passed through the filter and scanned for food particles.

Nutrient particles in the zooplanktons' environment are usually dispersed and patchy [3]. Hence, for a given organism successful feeding often happens randomly. Thus a good quantitative feeding performance metric should be independent of this randomness. Measuring the total volume of scanned fluid in one beating period can be a good metric for feeding performance without having further knowledge of how nutrients are dispersed. Such metrics have been used for study of feeding performance in current-feeding zooplankton [3–7]. If nutrients are well mixed such as by fast diffusion, all scanned fluid has the same probability of containing nutrients. However, such zooplankton often feed on micron-sized particles that do not diffuse on the length and time scales of feeding [2]. In that case, it is crucial to consider whether or not

<sup>&</sup>lt;sup>1</sup>University of Utah, Salt Lake City, UT, USA

<sup>&</sup>lt;sup>2</sup>University of Puget Sound, Tacoma, WA, USA

the scanned fluid has been previously filtered of prey by the organism. This requires information about the trajectories of all individual fluid particles in the domain during the past. In fluid mechanics, such a formulation of the flow field is called a Lagrangian description.

By contrast, it has been common in filter-feeding studies to examine the velocity field only at a certain area in space during a beating period [3,5–7], which is called a Eulerian description. Computationally, the Eulerian approach is more convenient than analysing trajectories of many fluid particles simulated over a long period of time. However, there is considerable variation in the literature as to how to define a correct Eulerian feeding metric. For example, Eulerian metrics used to study feeding performance in choanoflagellates [3,5–7], have differed in using near-field flows versus far-field flows, average geometries versus instantaneous geometries, and net flows versus inward flows passing through a filter.

Eulerian metrics typically do not provide any information on whether flows passing through the filter have been scanned before or not. In this work, we study feeding for an example organism to show that such previously scanned flows contribute a significant amount to the usual Eulerian metrics of feeding. We model feeding by *Vorticella*, an organism known for creating recirculatory flows around the cell [4,8,9], using both our experimental observations and information from the literature to generate a simplified geometry for the model. We used numerical simulations to compute the velocity fields and trajectories of food particles in the feeding current. Examining the trajectories of fresh food particles reveals that food capture preferentially occurs near the tip of cilia, which we corroborate via experimental observations. We create a Lagrangian feeding metric that measures only the fresh parts of the scanned fluid, and compare it with the results obtained from Eulerian metrics common in the literature. All the Eulerian metrics indicate a different amount of feeding from our Lagrangian metric, suggesting that feeding metrics for zooplankton cannot correctly be measured without taking into account whether fluid has been previously scanned.

## 2. Eulerian feeding metrics

As background we present some different ways that a Eulerian feeding metric can be constructed. Considering their limitations demonstrates why a Lagrangian feeding metric is necessary.

#### 2.1. Net flow metric

Downloaded from https://royalsocietypublishing.org/ on 22 April 2024

A most basic metric of feeding could be the net flow that passes through a filtering surface.

$$Q_1 = \int_0^T \int_A \mathbf{v}_{\text{rel}} \cdot \hat{\mathbf{n}} \, da \, dt, \tag{2.1}$$

where T is a beating period,  $\hat{\mathbf{n}}$  is the unit normal vector to the area element da and the spatial integral is performed over the filtering surface A. In this equation,  $\mathbf{v}_{\text{rel}} \cdot \hat{\mathbf{n}} \, da$  is the volume of fluid that passes through the area element da per unit time. This volume of fluid is positive if it moves in the direction of  $\hat{\mathbf{n}}$  and negative if it moves in the opposite direction, so flows in opposite directions cancel and  $Q_1$  measures a net flow through the filtering surface A. Therefore, this metric represents the volume of scanned fluid only in cases where we have a unidirectional flow (figure 1a), moving from one side of the filter to the other side of the filter at all times throughout the period. If flows go through the surface in opposite directions at different locations or at different times during the period (e.g. figure 1b), the metric will fail to compute the volume of scanned fluid accurately.

#### 2.2. Absolute flow metric

One way to deal with flows in opposite directions is to assign a positive value to all flows that pass through the filtering surface no matter which direction, i.e.

$$Q_2 = \int_0^T \int_A |\mathbf{v}_{\text{rel}} \cdot \hat{\mathbf{n}}| \, \mathrm{d}a \, \mathrm{d}t. \tag{2.2}$$

This metric will only work if each of the fluid particles passes through the filter only once (figure 1*b*). Otherwise multiple scanned fluid elements would be overcounted. Thus this metric cannot be used in cases where there are recirculatory flows through the surface (figure 1*c*).

#### 2.3. Inward flow metric

To prevent overcounting of recirculatory flows, past studies [5,6] have used an inward flow metric. In this metric an inward direction  $\hat{\mathbf{n}}$  for the surface is chosen in the predominant direction of the feeding current at the filtering surface (in the case of *Vorticella*, the inward direction is radially towards the central axis), and only area elements with flows going in that direction (i.e. satisfying  $\mathbf{v}_{\rm rel} \cdot \hat{\mathbf{n}} > 0$ ) are counted,

$$Q_3 = \int_0^T \int_{(\mathbf{v}_{rel} \cdot \hat{\mathbf{n}} > 0)} \mathbf{v}_{rel} \cdot \hat{\mathbf{n}} \, \mathrm{d}a \, \mathrm{d}t.$$
 (2.3)

However, even this metric does not completely solve the problem of recirculatory flows. Figure 1*d* shows three types of recirculatory flows: from top to bottom, a flow that recirculates over a long enough time such that nutrient particles are mixed into the flow far from the cell, a flow that recirculates within one period, and a flow that recirculates over more than one period. The inward flow metric

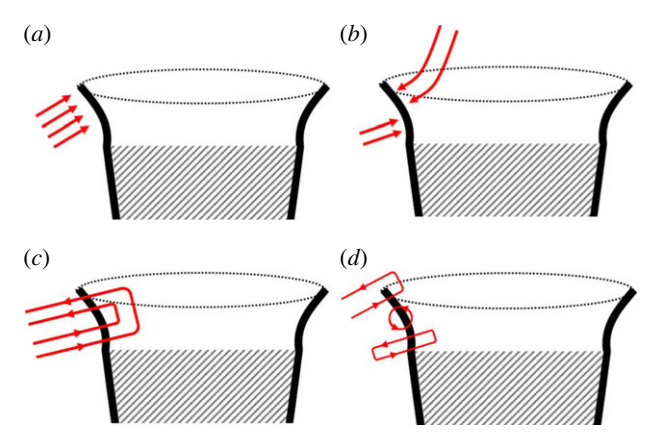


**Figure 1.** Schematic showing limitations of different Eulerian metrics. The upper part of an organism such as *Vorticella* is shown, with the filtering surface consisting of the black portions protruding above the shaded cell body. In all cases, we assume a steady flow with pathlines shown in red. (a) For a unidirectional flow, the net flow metric correctly computes the feeding performance. (b) For flows approaching the surface from different directions and no recirculations, the absolute flow metric correctly computes the feeding. (c) A scenario where the absolute flow metric fails and the net inward flow metric correctly computes the feeding. (d) Assuming three possible pathlines from top to bottom, a flow that recirculates over a long enough time such that nutrient particles are mixed into the flow far from the cell, a flow that recirculates within one period, and a flow that recirculates over more than one period. The inward flow metric incorrectly counts the latter two flows.

correctly accounts for the first flow but incorrectly counts the contribution of the other two flows, which should not contribute as they do not contain fresh nutrient particles.

#### 2.4. Time-averaged velocity fields in Eulerian metrics

We have defined the above metrics in equations (2.1)–(2.3) in terms of the instantaneous flow field relative to the surface  $\mathbf{v}_{\text{rel}}$ , leading to a volumetric flow over the instantaneous feeding surface in the inner integral, which is then averaged over one period of the feeding current. In the literature, Eulerian metrics often instead use velocity fields averaged over a period of the feeding current. Modelling time-dependent feeding flows by a steady flow [3,5] can be considered a type of time-averaged description.

Two assumptions exist for the filtering surface. The first supposes that it is time-independent, i.e. does not change position. For net flow metrics, using time-averaged velocities gives the same result as instantaneous velocities. In addition, one can often use the principle of mass conservation to equate the flow through a filtering surface with the flow through some other, more convenient, surface to observe experimentally, or calculate numerically, such as in [7,10]. However, for absolute and inward flow metrics, the instantaneous and time-averaged flows at a surface generally have different inward and absolute components [6]. Note that using a time-averaged flow instead of an instantaneous flow in an inward-flow metric can remove double-counting of flows that recirculate within one period, but still does not correctly account for flows that recirculate over more than one period. In addition, for absolute and inward flow metrics, it is usually not possible to use mass conservation to define a surface far from the filtering surface that will give equivalent results, since the definition of inward and absolute components is surface-dependent.

The second assumption supposes the filtering surface is time-dependent, i.e. moves over time. Again, the inward and absolute components of flow generally still differ between instantaneous and time-average flows. Additionally, if the filtering surface moves in time, then using average flow velocities comes with the added difficulty of defining an appropriate filtering surface to use in a Eulerian metric. While the average filtering surface position is a natural choice, for absolute and inward flow metrics there is no guarantee that it will give equivalent results to a metric using instantaneous velocities and filtering surfaces.

#### 2.5. Advection—diffusion models

Some works have incorporated filtering effects into a Eulerian framework by augmenting the flow model with an advection—diffusion model for the concentration field of nutrients or food particles [1,11–13]. In these models, filtration is accounted for by changing the boundary condition for the concentration field at the filtering surface. For example, perfect filtering would correspond to setting the concentration field to be zero at the filter. So far, however, it has not been quantified how much difference including filtering effects makes compared with other feeding metrics. We perform the comparison in this paper.

# 3. Experimental methods

We performed phase-contrast and dark-field microscopy on Vorticella samples purchased from the Carolina Biological Supply company. A sterilized wheat seed was added to the samples and they were maintained at 20°C for up to 10 days before observation. We used a Nikon Ti-E inverted microscope with  $40\times$  (phase contrast) and  $100\times$  (phase contrast and dark-field) magnifications. We placed a drop of the sample on a glass slide with a  $120\,\mu m$  thick spacer between the glass slide and the coverslip. We recorded videos (approx. 50 to approx. 500 frames per second (fps)) of Vorticella cells tethered to the coverslip with a Princeton Instruments Kuro2048 camera.

royalsocietypublishing.org/journal/rsif

J. R. Soc. Interface 21: 20230706

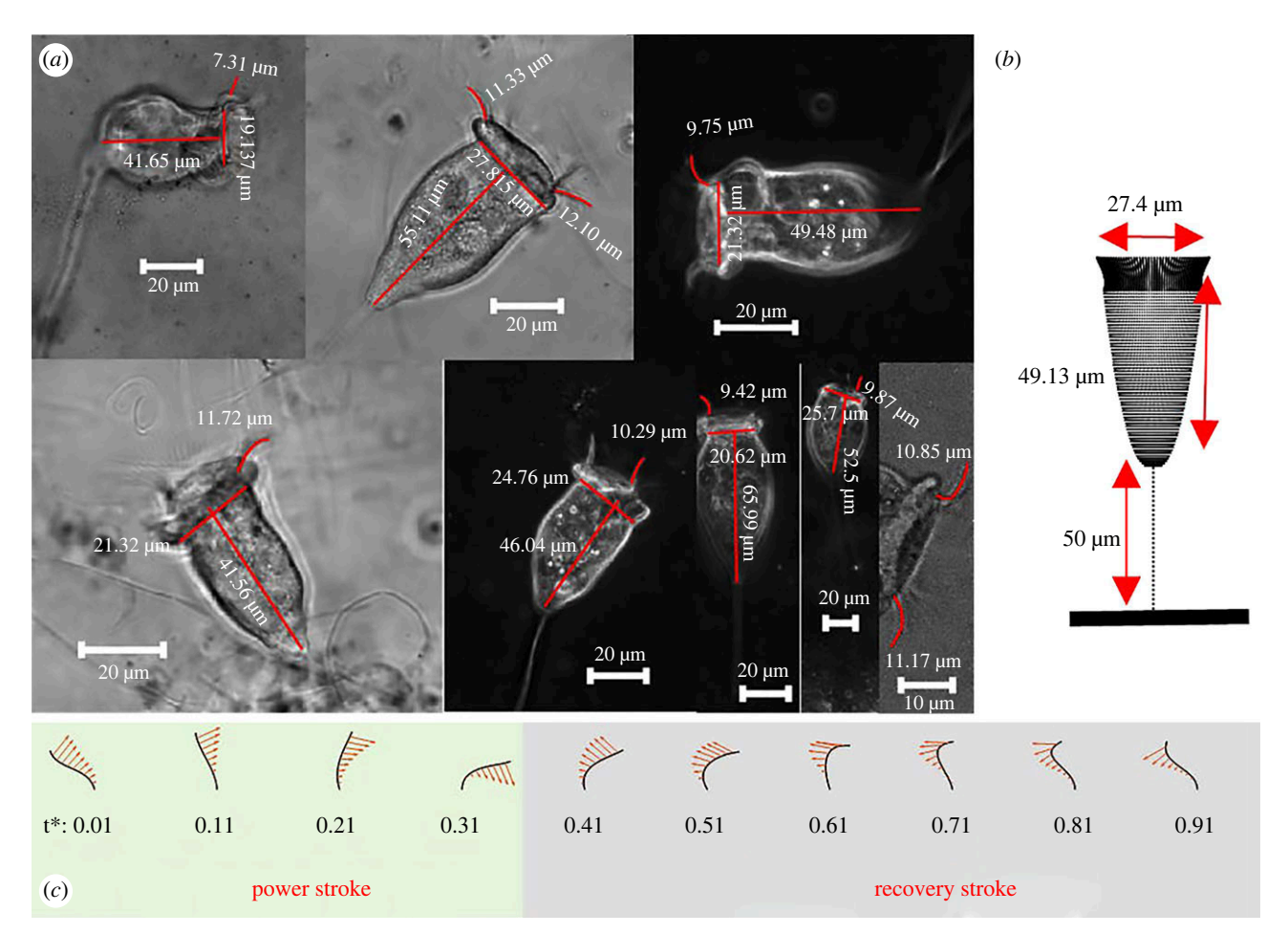


**Figure 2.** (a) Vorticella cells observed in laboratory. (b) Dimensions used for the model organism. Each point on the cell body and cilia represents a single regularized Stokeslet (see also figure 8). (c) Power stroke and recovery stroke phases of a cilium. The direction of the power stroke is radially outward.

We measured flow fields around Vorticella samples using micro-particle image velocimetry (PIV) by adding  $0.55 \, \mu m$  diameter spherical polystyrene particles (Spherotech Inc.) directly to the sample before observing it under the microscope using a  $40 \times$  objective. The polystyrene particles were first added to water and mixed well using a vortexer and subsequently added to the sample on the glass slide using a pipette. After adding the particles, the pipette tip was used to stir the sample on the glass slide. We used the Matlab toolbox PIV-Lab' to determine the flow fields from our videos [14]. For the micro-PIV analysis, we used 500 pairs of images using 1000 frames from the video. We used the contrast-limited adaptive histogram equalization (CLAHE) setting for the image pre-processing. A fast Fourier transform (FFT) window deformation method with two passes was used with an interrogation window size of 64 by 64 pixels and 32 by 32 pixels for each pass, respectively. The toolbox uses an ensemble correlation method. The dimensions of the image pairs used were 1452 pixels by 570 pixels. The pixel size was 0.11  $\mu$ m and the video frame rate was 85 fps.

A second set of experiments was performed to image the encounter location of food particles for *Vorticella*. We recorded videos of organisms attached to the bottom surface of a rectangular chamber (8 mm wide, 7 mm tall and 13 cm long) using a  $40 \times$  objective attached to a bellows (Nikon BD ELWD  $40 \times 0.5$  numerical aperture (NA), working distance 9.8 mm). This resulted in a field of view of  $522 \times 326 \,\mu\text{m}$ . Videos were recorded at  $1280 \times 800$  pixels at a frame rate of  $500 \,\text{fps}$  for  $10 \,\text{s}$  using a Phantom v. 210 camera. The water was seeded with  $5 \,\mu\text{m}$  neutral-density polyamide beads (Dantec Dynamics PSP-5) in order to track particle encounter and capture. Eleven individual *Vorticella* were observed, and all interactions with particles that were in focus were categorized based on the location of interaction—either at the tip (outer 25% of the cilium length) or the remainder of the cilium (inner 75% of the cilium). We observed a total of 295 particle interactions.

# 4. Vorticella geometry and feeding current

In our videos, we saw a bell-shaped geometry of the cell body (figure 2a) similar to those previously described in the literature [8]. Figure 2a shows observations of eight different cells and the estimated values for the bell length, bell width and cilium length. Values are obtained by manually choosing the start and end points of the red lines plotted on top of the images. We estimated the beating frequency to be approximately  $40 \, \text{Hz}$  and the maximum tip speed of a cilium to be  $900 \, \mu \text{m s}^{-1}$ .

Vorticella use an outer row of cilia positioned on the edges of the bell to generate flows and bring nutrient particles to their mouth-like peristome, where they use a second row of cilia to capture those nutrient particles [8,15]. The outer row of moving cilia undulates with a phase difference resulting in a metachronal wave [8]. From our observations, we were not able to precisely obtain the geometries of the cilia while beating (see electronic supplementary material, videos 1 and 2). However, we were able to determine the direction of the power stroke and recovery stroke of the cilia. In our videos, we saw that when the cilia were

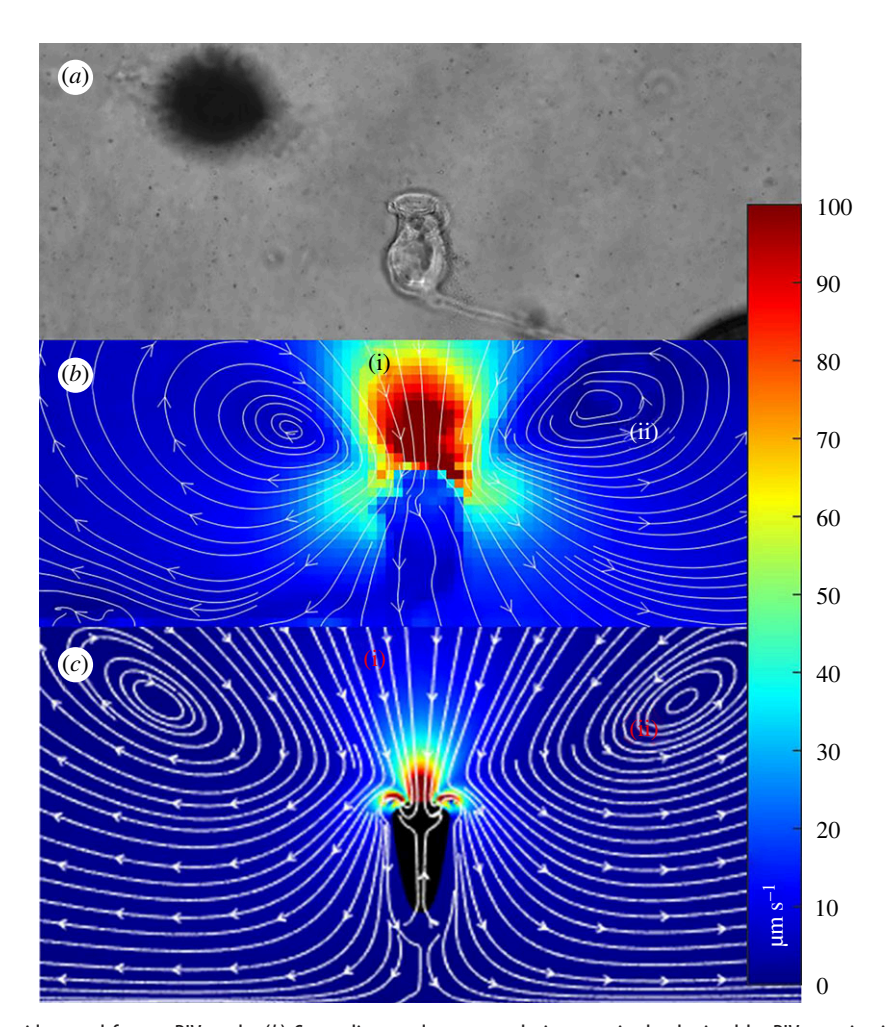


**Figure 3.** (a) A frame of the video used for our PIV study. (b) Streamlines and average velocity magnitude obtained by PIV examination of 500 pairs of frames. (c) Streamlines and average velocity magnitude were obtained using our numerical simulations with our model organism. All three images have the same scale and the larger dimension of the images is 400  $\mu$ m.

maximally curved, the tip of the cilia was farthest from the symmetry axis of the bell. Since a cilium is expected to be maximally curved towards the end of the power stroke, figure 2c suggests that the power stroke moves toward the outside of the bell.

PIV of the flow field around a *Vorticella* is shown in figure 3*b*. We observed two key characteristics: (1) a flow field moves towards the organism from above, presumably to bring nutrient particles from far away towards the peristome (labelled as (i) in figure 3*b*); (2) the existence of large recirculatory flows above and to the side of the cell (labelled as (ii) in figure 3*b*).

#### 5. Numerical methods

#### 5.1. Geometry used in numerical simulations

To study feeding metrics, we used an idealized geometry inspired by our observations of *Vorticella*. We chose our simplifying assumptions to reduce the required computations, while at the same time reproducing characteristics of the flow essential to feeding.

For our model, we assumed a bell-shaped body generated by the revolution of a quadratic curve, with a fixed distance to a wall (figure 2b). The dimensions are similar to those in figure 2a. We modelled the cell body using only a single surface on the outer surface of the bell shape, leaving a hollow (but closed on the bottom) interior, even though the cell body of actual *Vorticella* has significant material inside the bell and only a small gullet. The model has only one row of cilia on the edge of the bell, and all cilia beat together periodically instead of with a phase difference. This assumption simplifies computation since it removes the helical component of flow that appears when the cilia beat with a phase difference. The cilia are spaced 3° apart from each other relative to the central axis of the bell. This value was chosen because with this spacing, the maximum distance between adjacent cilia is smaller than 2 µm, the diameter of a typical bacterial prey. The simplifications made in our model are justified *a posteriori* by noting they reproduce the essential flow features of the feeding current (see next section).

Since we were not able to observe cilia kinematics for Vorticella, we used the kinematics reported for lung cilia [16],

$$\mathbf{r}(s,t) = \frac{1}{2}\mathbf{a}_{0}(s) + \sum_{n=1}^{N_{0}} \mathbf{a}_{n}(s)\cos n\omega t + \mathbf{b}_{n}(s)\sin n\omega t, \tag{5.1}$$

where *s* changes from 0 to the length of the cilium arc length, *t* is time,  $\mathbf{r}(s, t)$  is position of points on the cilium,  $\omega = 2\pi \times 40 \,\text{Hz}$  is the beating frequency, and  $\mathbf{a}_n$  and  $\mathbf{b}_n$  are Fourier coefficients provided in appendix A. Figure 2*c* shows the shape of a cilium at 10 different instances during a period.

**Figure 4.** (a,b) Schematic showing the surface used for the Lagrangian metric; we picked an imaginary surface that encloses the cilium one prey radius away from it. Prey particle is depicted in red in (b). Since the cilium moves throughout the period, the surface also moves. (c-e) Different possible trajectories: (c) fresh particle (d) non-fresh particle part of a large recirculation that has passed through the surface several periods ago (each dot is the position of the particle after one period), (e) non-fresh particle part of a small recirculation within one period. In (b-e), the cilium shown is on the right-hand side of the cell, i.e. the interior of the cell is towards its left.

#### 5.2. Calculation of velocity field using the method of regularized Stokeslets

At the length scales of our problem, flows are dominated by viscous effects rather than inertial effects, and therefore are described by a low Reynolds number ( $Re \approx 10^{-2}$ ). Hence, for an incompressible Newtonian fluid, the velocity field  $\mathbf{u}(\mathbf{x}, t)$  and pressure field  $p(\mathbf{x}, t)$  obey the Stokes equation

$$-\nabla p + \mu \nabla^2 \mathbf{u} + \mathbf{f}(x, t) = 0 
\nabla \cdot \mathbf{u} = 0,$$
(5.2)

where  $\mu$  is the dynamic viscosity of the fluid, and f is a force distribution exerted by the organism's surface on the fluid. In our simulations, we represent the organism by discretized points on its surface, assuming each is exerting a force on the fluid. Figure 2b shows the discretized points on the surface of the organism, and appendix A explains the details of the discretization. We approximate each point force with a regularized force density via the method of regularized Stokeslets [17,18], with images [19] to account for the wall boundary. Details of our implementation, which we have previously reported [20–22], are in appendix B. In this method, we find the velocity field such that it is zero on the wall and for discretized points on the stationary *Vorticella* bell, and equal to the prescribed velocity of the beating cilia for the discretized points on the cilia.

We discretize one beating period into 100 time steps and we obtain the velocity field  $\mathbf{u}(\mathbf{x}, t)$  at each time step using the above method. Figure 3c shows the resulting velocity field averaged over one period. Qualitatively, the simulated flow field reproduces the essential features we observed, flows coming from above towards the mouth (figure 3c(i)) and recirculatory flows (figure 3c(ii)). The direction of the power stroke inferred from our observations was validated since it produced feeding flow moving towards the cell from above; reversing the direction of the power stroke produced upward flows instead. While the velocity fields qualitatively agree, comparison of (b) and (c) in figure 3 shows that there is a quantitative discrepancy between the velocity magnitudes. For example, one cell length (50  $\mu$ m) above the cell, the magnitude of averaged fluid velocity is 74  $\mu$ m s<sup>-1</sup> in the experiment and 27.8  $\mu m s^{-1}$  in the simulation. This discrepancy could arise from differences in the number of cilia, number of rows of cilia, and the cilia beating pattern in our model compared with the real organism. Furthermore, our model organism is perpendicular to one nearby boundary while in our micro-PIV experiments, the cells are parallel to boundaries; it is known that the angle between a Vorticella cell and nearby boundaries, the proximity of the boundaries and the number of boundaries affects the size of recirculatory flows [9,23]. Nonetheless, our model organism succeeds in capturing the qualitative features of recirculatory feeding flows. We will see that the direction of feeding flow and the presence of recirculation greatly affect the accuracy of Eulerian compared with Lagrangian feeding metrics. Since our model flow has such recirculatory features, we consider it to be suitable for studying the relative merit of these metrics. This also justifies the simplifications we made to the cell body and cilia geometries, and ciliary beating kinematics.

#### 5.3. Lagrangian feeding metric

Downloaded from https://royalsocietypublishing.org/ on 22 April 2024

In this work, we assume the cilia form a filtering surface (shown in blue in figure 4a) and the process of filtering nutrients in *Vorticella* happens immediately when a particle makes contact with this surface.

A typical prey particle is assumed to be a sphere with the radius of 1  $\mu$ m. All points in space that are one radius away from the filter form an enclosing surface around the filter as shown in figure 4a. A close-up of the enclosing surface for a single flagellum is shown in figure 4b, with the prey particle shown in red. Our Lagrangian feeding metric is the total volumetric flow through this enclosing surface, but considering only flows that have not been scanned before,

$$Q_{\text{Lag}} = \int_{0}^{T} \int_{\Phi} (\mathbf{v}_{\text{rel}} \cdot \hat{\mathbf{n}} \, da) \, dt, \tag{5.3}$$

where  $\Phi$  denotes parts of the enclosing surface where this condition is satisfied. To determine which flows have been scanned, we obtain the history of fluid particles that have reached the enclosing surface. We do this by propagating their trajectories backward in time and checking their distance from the filtering surface. A similar idea is implemented in [23,24] for a simpler model of *Vorticella*.

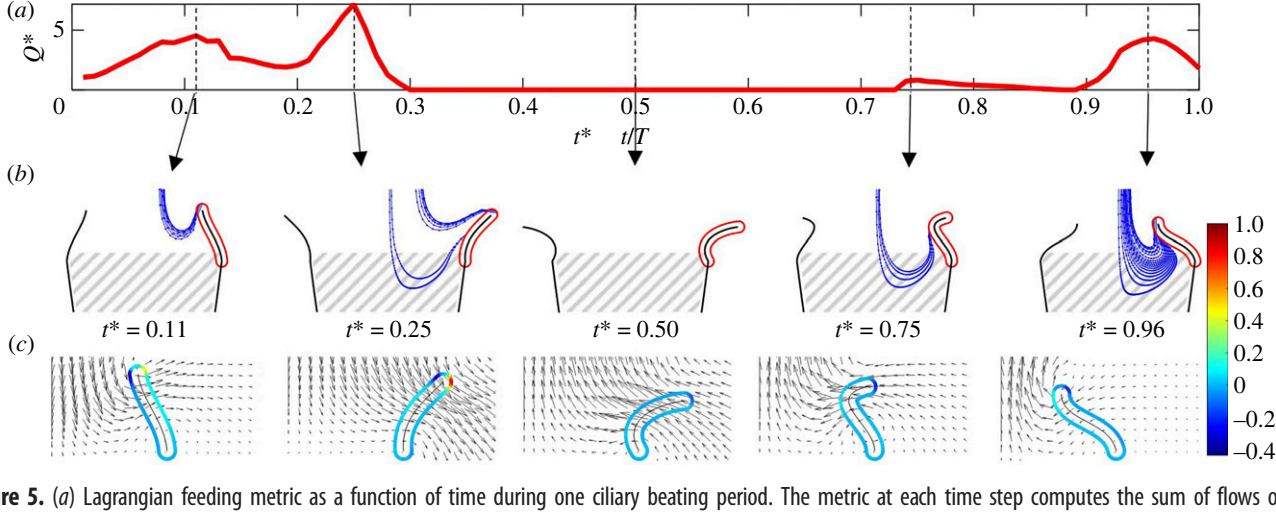


**Figure 5.** (a) Lagrangian feeding metric as a function of time during one ciliary beating period. The metric at each time step computes the sum of flows on the enclosing surface that contain fresh nutrient particles. Dimensionless flows are  $Q^* = Q/Q_0$ , where  $Q_0$  is the net flow rate through the average filtering surface averaged over one period (see equation (6.1) and accompanying text). Times on the *x*-axis are normalized by one period,  $t^* = t/T$ . (b) Trajectories of fresh fluid particles (blue) that reach the enclosing surface (shown in red) one prey radius away from the cilium. Trajectories are plotted for six sample instances during the period. Each trajectory is traced back for 300 periods. (c) Instantaneous velocity field and positioning of cilia. The colours show the absolute flux on different parts of the enclosing surface and are normalized by the maximum flux throughout the period.

To simplify the simulations, we assume all cilia move in phase, not in a metachronal wave. Due to the symmetry of the beating cilia, particle trajectories stay in a single azimuthal plane. To reduce the number of trajectories computed, we only examined particles in a plane that passes through the middle of two adjacent cilia. In this plane, we calculate the backward trajectory of Lagrangian particles that originate at 106 equally spaced positions on the enclosing surface (details in appendix C and figure 8).

For a given particle at position  $x_i$  at time  $t_n = n \times \Delta t$ , we obtain the particle's previous position  $x_{i-1}$  using the calculated fluid velocity  $U_i(x_i)$ 

$$\mathbf{x}_{i-1} = \mathbf{x}_i - \mathbf{U}_i(\mathbf{x}_i) \times \Delta t. \tag{5.4}$$

Since the flow is not steady and the feeding surface moves, we need to consider particles originating at the enclosing surface at all times during the period.

Figure 4c,d,e shows example pathlines of fresh and non-fresh flows that end up on the enclosing surface.

# 6. Lagrangian feeding metric

Downloaded from https://royalsocietypublishing.org/ on 22 April 2024

Figure 5a shows the time-resolved Lagrangian feeding metric calculated for one beating period of the cilia. The flow is normalized by  $Q_0$ , the net flow rate through the average filtering surface averaged over one time period,

$$Q_0 = \frac{1}{T} \int_{A_{\text{avg}}} \int_0^T \mathbf{v} \cdot \hat{\mathbf{n}} \, dt \, da, \tag{6.1}$$

where the average filtering surface  $A_{\text{avg}}$  is defined by the time-averaged position of the cilia. Both the time-averaged cilia position and the average flow rate are shown in figure 6. Note that due to mass conservation,  $Q_0$  is also equal to the average flow rate through the horizontal circular surface above the mouth of the *Vorticella* bounded by the edge of the average filtering surface. In our model organism, for a beating frequency of  $40 \, \text{Hz}$ ,  $Q_0 = 1.45 \times 10^{-14} \, \text{m}^3 \, \text{s}^{-1}$ .

By examining the feeding metric and filtering surface at each time, we can determine which regions of the surface scan fresh nutrient particles, and how the feeding current brought those particles to the filtering surface. The peaks in figure 5a correspond to times when a larger portion of flows reaching the surface are actually fresh.

Figure 5b shows the enclosing surface at example instances during the period, and past trajectories of fresh particles that touch the filtering surface at those instances. Figure 5c shows the instantaneous velocity field and the positioning of the filtering surface at those moments. The colours show the flux  $(\mathbf{u}_{rel} \cdot \hat{\mathbf{n}})$  at different sections of the enclosing surface. The flux values on all sections and at all times are normalized by the same maximum value during the period.

# 7. Implications for feeding mechanism

Together, these figures give a more detailed understanding of the feeding mechanism. First, we see that most of the fresh feeding happens during the power stroke phase of the cilia ( $t^* = 0$  to  $t^* = 0.4$ ). Second, we see that during this time, most of the fresh nutrient particles first make contact with the filtering surface at the tip region. By contrast, during the recovery stroke when we have lower feeding rates, we see that there are many fresh particles that reach the filtering surface around its middle inner region ( $t^* = 0.75$  and  $t^* = 0.96$ ).

**Figure 6.** (a) Averaged geometry of one cilium over one beating period and the averaged velocity field in the beating plane of that cilium (shown only on right-hand side of the cell). (b) A detailed view of the averaged velocity field near the averaged cilium shows that most of the flow is entering the surface from right to left.

**Table 1.** Table showing the number and location of first-time contact interactions of particles with Vorticella cilia in our experiments.

first interaction at tip (outer 25% of a cilium)	271 (92%)
first interaction at the inner section of the cilium	24 (8%)

This pattern of fresh particles is partially explained by where most of the fluid flows through the filtering surface. Examining the instantaneous flux going through the filtering surface in figure 5c, we see that there are larger inward fluxes during the power stroke phase, and that these larger inward fluxes happen around the tip of the filtering surface. However, note that even though nearly the entire surface has inward flow through it, most of the fresh flow is only at the tip. Thus it is crucial to distinguish the flows through the filtering surface that contain fresh particles.

To experimentally corroborate these insights from our numerical model, we examined videos of feeding vorticella obtained as described in §3. We manually examined the trajectories of particles that move towards *Vorticella* cells in our experimental data. We categorized the detected trajectories based on whether they first interact with a cilium at its tip (i.e. outer 25% of cilium) or its inner section (see electronic supplementary material, videos 3–6 for examples). Table 1 shows the percentages of occurrence of each group. We see that about 92% of first interactions occur at the tip. Regardless of where the first interaction occurs, about half the time we saw that it results in a capture. We assumed a capture happens when a particle is guided by the cilia towards the mouth and becomes unidentifiable in the video after a while.

Finally, by examining the trajectories of the nutrient particles that reach the filtering surface, one can identify from which regions of space the organism is obtaining nutrients. This is possible only when using a Lagrangian metric. For example, in figure 5b, we see that all fresh particles reach the surface from directly above the centre of the cell, highlighting that region as of particular importance for feeding. Such information could potentially improve estimates of feeding based on far-field experimental PIV observations, as in [4].

# 8. Comparison of feeding metrics

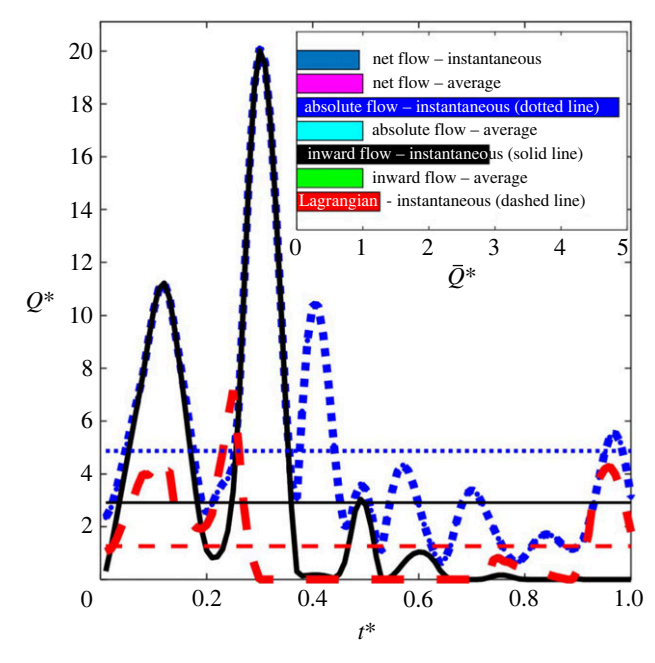
Downloaded from https://royalsocietypublishing.org/ on 22 April 2024

Figure 7 shows the results of using our new Lagrangian metric along with various Eulerian metrics for our example organism. The Eulerian metrics that we computed for comparison can be put in two main groups: (i) the ones that are computed using instantaneous velocities and using a moving filtering surface throughout the period, and (ii) the ones that are computed using averaged values of the velocity and on a filtering surface generated from an averaged geometry of the organism throughout the period. The instantaneous metrics are plotted in thick lines as a function of time, with their time-average values throughout the period plotted with the same colour but with thin horizontal lines. In the inset, these time-averaged values are plotted again in addition to the metrics computed using averaged velocities. The Lagrangian metric itself is plotted with a red dashed line.

First, we discuss the volumetric net flow (equation 2.1, magenta in figure 7 inset) that passes through the filtering surface determined by the cilia. This metric is similar to the metric used in [7], which is a good choice in that problem since they have a unidirectional flow going from one side of their 'encounter zone' to the other side. However, in our problem, we see that it is smaller than the Lagrangian metric on average, since our flow is not unidirectional, and flows going through the filtering surface in opposite directions cancel each other out.

Next, consider the absolute flow metric (equation 2.2), which computes all flows that pass through the filtering surface regardless of direction. The absolute flow metric using instantaneous values of velocity (blue dotted line in figure 7) is expected to yield the highest values for feeding compared with other metrics, since it counts all the flows that pass through the filtering surface at all times and nothing is cancelled out. In the figure we see this, the blue bar is significantly larger than other metrics. The absolute flow metric using averaged velocities and an averaged geometry (cyan in figure 7 inset) yields significantly different results from instantaneous flows. We also see that it is different from the time-averaged Lagrangian metric, and it still has the largest value of the time-averaged metrics.

The inward flow metric (equation 2.3) computes all flows that pass through the filtering surface only in one direction. Here, we have chosen the inward direction to be pointing radially towards the symmetry axis of the bell from the larger radius to the smaller radius. The inward flow using instantaneous velocity fields (black solid line in figure 7) is significantly different from our Lagrangian



**Figure 7.** Various metrics of feeding performance computed using a Eulerian approach (§2) for our model organism compared with the Lagrangian metric. Metrics that are computed throughout the period are plotted as a function of time. The *x*-axis is the time during one beating period of cilia, the *y*-axis shows different flows non-dimensionalized. The inset shows the average values of these instantaneous metrics, as well as three other metrics that are computed using average values during one beating period. All flows are non-dimensionalized by the net flow computed using average velocities and average filtering surface (magenta bar). The figure shows that, first, the Eulerian metrics yield very different results from one another, and, second, neither of them are equal to the correct Lagrangian metric.

metric. We also see that during the power stroke phase ( $t^* < 0.4$ ), it is very similar to the absolute flow metric, showing that during the power stroke most of the flow is passing through the filtering surface from outside towards the inside, while during the recovery stroke most of the flow is passing through the filtering surface in the opposite direction. The inward flow metric using time-averaged velocity fields and geometry (green in figure 7 inset) also has a different value from our Lagrangian metric but is only slightly smaller than the average version of the absolute flow. This is explained by looking at the averaged velocity field and the averaged geometry in figure 6, which shows that most of the averaged flow enters the averaged enclosing surface from the outer half, so that it is counted in both the inward and absolute flow metrics. Our time-averaged inward flow metric is similar to the one used in [5,6]; in those studies having a unidirectional averaged flow makes the choice more justified than in this problem.

In conclusion, figure 7 indicates that the different metrics we have computed yield very different results from each other and from the correct Lagrangian metric as well.

#### 9. Discussion

In this work, we used a simplified model inspired by *Vorticella* to show that a Lagrangian feeding metric, that only takes into account fluid which has not been previously scanned, yields different results for the feeding ability compared with commonly used Eulerian metrics. Determining which fluid has already been scanned requires examining the past trajectories of fluid material that contacts the filtering surface. The trajectories and experimental observations of feeding also indicate that *Vorticella* captures food predominantly at the tips of its cilia. Accurate analysis of these trajectories requires time-resolved, rather than period-averaged velocity fields and filtering surfaces. Our results suggest that one should carefully justify the use of Eulerian metrics when quantifying feeding efficacy of feeding currents, especially when recirculatory flows are present. If filtered volumes are incorrectly estimated, it could lead to erroneous conclusions about feeding rates, nutrient requirements, or energy expenditures of feeding organisms.

Our comparison between the Lagrangian and Eulerian metrics also reinforces when Eulerian metrics may lead to adequate assessments of feeding efficacy. If the flow through the filtering element is mostly in one direction then net, absolute and inward metrics will all be similar. However, they will only be close to a Lagrangian metric if there is little recirculation. Eulerian metrics that use average flow can be close, but not exactly the same as a Lagrangian metric if most of the recirculation occurs within one period due to oscillatory beating patterns, with little recirculation over long time scales. This is the case in our *Vorticella* example, for which the absolute and inward flow metrics that use average flows and filtering locations are both only 20% different from the Lagrangian metric. Thus in some cases, more easily measured or calculated Eulerian metrics could be used to speed up the assessment of feeding efficacy in systems with well-characterized feeding currents. However, in general for feeding current flows that are not well-understood, there is no guarantee that they are similar, or a way to quantify how much the Eulerian and Lagrangian metrics differ, without calculating each of the metrics first.

Although this Lagrangian approach to quantifying feeding may be more accurate than the Eulerian approaches, it is considerably more difficult to calculate since it requires time-dependent flows and trajectories. Experimentally, it is also much more difficult to study these spatially and temporally resolved flows, when compared with time-averaged fluxes. This study thus highlights the need for simplified ways to calculate and measure accurate feeding metrics.

**Figure 8.** We generated the enclosing surface by incorporating four curves. (i) and (ii) are the cilium that are horizontally translated one prey radius away. (iii) and (iv) are two semi circles with radius equal to one prey radius. We used this enclosing surface to obtain final positions of the Lagrangian particles and to generate area elements.

Finally, our study has assumed that food particles do not diffuse on the time scales relevant to their advection in feeding currents. It could be improved by including such diffusive effects, which may become important for smaller food particles or large flow structures. For example, if in a large recirculatory flow, there is enough time for new food to diffuse into the current, then our metrics would undercount feeding efficacy. The advection–diffusion models discussed in §2.5 provide a way to incorporate diffusion of food, and also take into account the history of whether fluid has previously been scanned by the filter. However, they do require an additional step of solving the advection–diffusion equation in addition to calculating the velocity field.

Ethics. This work did not require ethical approval from a human subject or animal welfare committee.

Data accessibility. The data and codes used for this research are available from the Zenodo repository: https://zenodo.org/records/10601122 [25]. Supplementary material is available online [26].

Declaration of Al use. We have not used AI-assisted technologies in creating this article.

Authors' contributions. K.S.: data curation, formal analysis, software, validation, visualization, writing—original draft; L.S.A.: data curation, writing—review and editing; H.R.: data curation; R.S.: funding acquisition, methodology, supervision, writing—review and editing; R.E.P.: data curation, writing—review and editing; H.C.F.: conceptualization, formal analysis, funding acquisition, investigation, methodology, project administration, supervision, writing—review and editing.

All authors gave final approval for publication and agreed to be held accountable for the work performed therein.

Conflict of interest declaration. We declare we have no competing interests.

Funding. K.S., L.S.A., R.S. and H.C.F. were supported by National Science Foundation grant no. CBET-1805847. K.S. was also supported by National Science Foundation grant no. CMMI-2027417. R.E.P. was supported by National Science Foundation grant no. IOS-1755326.

Acknowledgements. We thank Anders Andersen, Thomas Kiørboe and Lasse Tor Nielsen for use of facilities and help with particle encounter experiments.

# Appendix A. Parameters used in the simulations

For the dynamic viscosity of water, we have used the value  $\mu = 0.001$  Pa s. We assumed the angular beat frequency of the cilia is  $\omega = 1$  rad s<sup>-1</sup> and its beating period is  $T = 2\pi/\omega$ . We assumed the cell is attached to wall with a fixed distance that we chose to be d = 50 µm.

We chose the cilium arc length to be  $10 \, \mu m$  and its geometry as a function of time is represented by equation (5.1) based on data from [16]. We assume each cilium filament is 200 nm thick [15,27,28]. We discretize each cilium filament with 50 Stokeslets along its centreline. We use a regularization parameter of Stokeslets on the cilia of  $\epsilon = 200 \, nm$  to represent its thickness. This also sets the spacing between Stokeslets, so the distance from each Stokeslet always has a 200 nm distance with its adjacent Stokeslets [21].

We generated the bell by rotation of a quadratic curve around the symmetry axis of the bell. We discretize the quadratic curve with 60 points with an equal distance between adjacent points along the curve. For the curve, we used the equation  $y = x^2/3.125$  for  $0 \le x \le 12.5$  µm, where x and y are in units of micrometre, which results in the arc length of the curve to be 52.558 µm and its height to be 49.131 µm. We put one cilium filament at the tip of this curve. We translated this curve and its corresponding cilium horizontally (in the x-direction) by  $r_{\text{base}} = 1.5$  µm from the origin and then rotated it by 3° increments around the symmetric axis of the bell resulting in  $120 \times 60 = 7200$  Stokeslets on the bell and  $120 \times 50 = 6000$  Stokeslets for the cilia filaments. We chose the  $\Delta\theta = 3^\circ$  value so that, for a typical bacterial prey diameter of 2 µm, the distance between the tips of two adjacent cilia are smaller than that diameter. For the Stokeslets on the bell, we chose their regularization parameter as  $\epsilon = 2r\Delta\theta$ , where r is the radial distance of the Stokeslet from the symmetry axis. We discretized the surface of the circle at the base of the bell with 32 uniformly distributed Stokeslets and used the regularization parameter  $\epsilon = r_{\text{base}}/5$  for them. The resulting discretization is shown by the points in figures 2b and 8.

For the cilia stroke, the Fourier coefficients  $\mathbf{a}_n$  and  $\mathbf{b}_n$  in equation (5.1) are vector quantities and their values are obtained using the data in [16]. They are approximated by

$$\mathbf{a}_{n} = \sum_{m=1}^{3} \mathbf{A}_{mn} s^{m}$$

$$\mathbf{b}_{n} = \sum_{m=1}^{3} \mathbf{B}_{mn} s^{m},$$
(A 1)

and

Downloaded from https://royalsocietypublishing.org/ on 22 April 2024

where s changes from zero to the arc length of a cilium and  $A_{mn}$  and  $A_{mn}$  are given in table 2(B) of [16].

royalsocietypublishing.org/journal/rsif J. R. Soc. Interface 21: 20230706

### Appendix B. Method of images for regularized Stokeslets

If we have a point-force at  $x_0$ ,  $f(x, t) = f(t)\delta(x - x_0)$ , with  $\delta(\mathbf{r})$  being the Dirac delta function, the Stokeslet velocity field  $\mathbf{u}^s$  that satisfies the Stokes flow in equation (5.2) is given by

$$u_i^s(\mathbf{x}) = \sum_j G_{ij}(\mathbf{x}, \mathbf{x}_0) f_j, \tag{B1}$$

where  $i, j = \{1, 2, 3\}$  are indices that denote x, y, z components, so that (for example)  $u_i^s$  are the components of the Stokeslet velocity field. Further, the kernel **G** is a second-rank tensor with components

$$G_{ij}(\mathbf{r}) = \frac{1}{8\pi\mu} \left( \frac{\delta_{ij}}{|\mathbf{r}|} + \frac{r_i r_j}{|\mathbf{r}|^3} \right),\tag{B2}$$

where  $\delta_{ij}$  is the Kronecker delta, and  $\mathbf{r} = \mathbf{x} - \mathbf{x}_0$ . Due to the linearity of the Stokes equation, the resultant fluid velocity at point  $\mathbf{x}$  due to several point forces is given by the superposition of the flows of each one of those forces individually. Such a superposition can be used to generate the flow velocity field around complex geometries such as our *Vorticella* model.

However, the representation of flows using the Stokeslet above is complicated by the singularity at  $|\mathbf{r}| = 0$  in equation (B 2). In the method of regularized Stokeslets [17,18], in order to avoid the singularity at  $\mathbf{x} = \mathbf{x}_0$ , the Dirac delta function is approximated by a smooth radial function  $\Psi_{\epsilon}(r)$  such that  $\int_0^\infty r^2 \Psi(r) \, dr = 1$ . The details for choosing  $\Psi_{\epsilon}(r)$  and modifying the method for flows in the presence of a wall are given in [19]. Here, the key fact is that  $\mathbf{G}(\mathbf{r})$  is replaced by a new kernel,  $\mathbf{G}^I(\mathbf{r}, \epsilon)$ , which maintains the noslip boundary condition on the wall and now also depends on the regularization parameter  $\epsilon$ . The exact formula for  $\mathbf{G}^I$  that we use can be found in eqn (21) of [19]. A more lengthy description of our implementation of the method of regularized Stokeslets can be found in [21], but briefly, the fluid velocity  $\mathbf{u}(\mathbf{r})$  at position  $\mathbf{r}$  in the domain and in the presence of a wall at the plane x = 0, resulting from N regularized forces at positions  $\mathbf{R}^b$  each having a force  $\mathbf{f}^b$  and regularization parameter  $\epsilon^b$  is

$$u_i(\mathbf{r}) = \sum_{\substack{b = 1, \dots, N \\ j = 1, \dots, 3}} G_{ij}^I(\mathbf{r} - \mathbf{R}^b, \boldsymbol{\epsilon}^b) f_j^b.$$
(B3)

At the positions of the N regularized forces themselves ( $\mathbb{R}^{a}$ ), the fluid velocity field is

$$u_i(\mathbf{R}^a) = \sum_{\substack{b = 1, \dots, N \\ j = 1, \dots, 3}} G^I_{ij}(\mathbf{R}^a - \mathbf{R}^b, \boldsymbol{\epsilon}^b) f^b_j.$$
(B4)

The no-slip boundary condition requires that the fluid velocities in equation (B 4) are equal to the prescribed velocity of the surface of our *Vorticella* organism. In our simulations, we assume the cell is fixed in the space with a constant distance from the wall, and we know the positions of Stokeslets on the beating cilia at any time since we have the beating representations as a function of time. Based on this, we obtain the velocity of each Stokeslet on a cilium by the difference in its position from the time step prior to the current instance and the time step after the current instance. For the rest of the Stokeslets, their velocities are set equal to zero. Knowing these velocities, equation (B 4) becomes a linear equation which can be inverted to solve for the forces  $\mathbf{f}^b$ . Then, knowing  $\mathbf{f}^b$ , equation (B 3) gives the velocity field at all positions in space, i.e. the complete feeding current.

# Appendix C. Details of numerical implementation of Lagrangian metric C.1. Time steps

In our simulations, we used the time step  $\Delta t = 0.01T$ , where T is the beating period. We checked that reducing the time step to  $\Delta t = 0.005T$  results in negligible difference (less than %1 in number of detected trajectories of fresh particles).

#### C.2. Final position of Lagrangian particles

We used an enclosing surface around and one prey radius away from a cilium and discretized that surface to obtain the starting position of our Lagrangian particles in our simulations.

In order to generate the enclosing surface around the cilium, we used four curves. We translated the cilium horizontally one prey radius towards the symmetry axis (figure 8(ii)), and one prey radius away from the symmetry axis (figure 8(ii)). Additionally, we used two semicircles with the radius equal to a prey radius and centres located at the starting point and the endpoint of the cilium (figure 8(iii) and (iv)). We discretized this enclosing surface with points that separated 0.25 µm from each other, obtaining 106 points along the surface. In our simulations, we assumed these 106 points to be the final position of our Lagrangian particles and we propagated their trajectories backward in time. In this way, we calculated trajectories of particles in one azimuthal plane that end up touching the cilium. On the left, each point on the cell body and cilia shows the location of a regularized Stokeslet. On the right, each point shows one of the 106 final positions for food particles touching the cilium.

#### C.3. Area elements for volumetric flux calculations

We calculated the flux in equation (5.3) by summing over fluxes through area elements described below. We assumed each of the discretized points  $\mathbf{p}_b$  with b = 1, ..., 106 are also at the centre of a line element, and that a corresponding area element is made by

royalsocietypublishing.org/journal/rsif

the 360° rotation of that line element around the *y*-axis. The area of that element is obtained as  $a_b = 2\pi \times R_b \times \Delta h_b$ , where  $R_b$  is the radial distance of  $\mathbf{p}_b$  from the symmetry axis and  $\Delta h_b$  is the length of the line element. Additionally, we obtained the vector normal to the area element by rotating the unit vector parallel to the line element by 90°.

#### References

- Short MB, Solari CA, Ganguly S, Powers TR, Kessler JO, Goldstein RE. 2006 Flows driven by flagella of multicellular organisms enhance long-range molecular transport. Proc. Natl Acad. Sci. USA 103, 8315–8319. (doi:10.1073/pnas.0600566103)
- 2. Kiørboe T. 2011 How zooplankton feed: mechanisms, traits and trade-offs. Biol. Rev. 86, 311-339. (doi:10.1111/j.1469-185X.2010.00148.x)
- 3. Roper M, Dayel MJ, Pepper RE, Koehl MAR. 2013 Cooperatively generated stresslet flows supply fresh fluid to multicellular choanoflagellate colonies. *Phys. Rev. Lett.* **110**, 5. (doi:10.1103/PhysRevLett.110.228104)
- 4. Nagai M, Oishi M, Oshima M, Asai H, Fujita H. 2009 Three-dimensional two-component velocity measurement of the flow field induced by the *Vorticella picta* microorganism using a confocal microparticle image velocimetry technique. *Biomicrofluidics* **3**, 014105. (doi:10.1063/1.3105106)
- 5. Kirkegaard JB, Goldstein RE. 2016 Filter-feeding, near-field flows, and the morphologies of colonial choanoflagellates. Phys. Rev. E 94, 7. (doi:10.1103/PhysRevE.94.052401)
- Nguyen H, Koehl MAR, Oakes C, Bustamante G, Fauci L. 2019 Effects of cell morphology and attachment to a surface on the hydrodynamic performance of unicellular choanoflagellates. J. R. Soc. Interface 16, 20180736. (doi:10.1098/rsif.2018.0736)
- 7. Andersen A, Kiørboe T. 2020 The effect of tethering on the clearance rate of suspension-feeding plankton. Proc. Natl Acad. Sci. USA 117, 30 101–30 103. (doi:10.1073/pnas.2017441117)
- 8. Sleigh MA, Barlow D. 1976 Collection of food by Vorticella. Trans. Am. Microsc. Soc. 95, 482. (doi:10.2307/3225140)
- Pepper RE, Roper M, Ryu S, Matsudaira P, Stone HA. 2010 Nearby boundaries create eddies near microscopic filter feeders. J. R. Soc. Interface 7, 851–862. (doi:10.1098/rsif. 2009.0419)
- 10. Nielsen LT, Asadzadeh SS, Dölger J, Walther JH, Kiørboe T, Andersen A. 2017 Hydrodynamics of microbial filter feeding. *Proc. Natl Acad. Sci. USA* **114**, 9373–9378. (doi:10.1073/pnas.1708873114)
- 11. Asadzadeh SS, Nielsen LT, Andersen A, Dölger J, Kiørboe T, Larsen PS, Walther JH. 2019 Hydrodynamic functionality of the lorica in choanoflagellates. *J. R. Soc. Interface* **16**, 20180478. (doi:10.1098/rsif.2018.0478)
- Asadzadeh SS, Kiørboe T, Larsen PS, Leys SP, Yahel G, Walther JH. 2020 Hydrodynamics of sponge pumps and evolution of the sponge body plan. eLife 9, e61012. (doi:10.7554/eLife.61012)
- Asadzadeh SS, Walther JH, Kiørboe T. 2023 Conflicting roles of flagella in planktonic protists: propulsion, resource acquisition, and stealth. PRX Life 1, 013002. (doi:10.1103/PRXLife.1.013002)
- 14. Thielicke W, Sonntag R. 2021 Particle image velocimetry for MATLAB: accuracy and enhanced algorithms in PIVIab. J. Open Res. Softw. 9, 12. (doi:10.5334/jors.334)
- 15. Ryu S, Pepper R, Nagai M, France D. 2016 Vorticella: a protozoan for bio-inspired engineering. Micromachines 8, 4. (doi:10.3390/mi8010004)
- Fulford G, Blake J. 1986 Muco-ciliary transport in the lung. J. Theor. Biol. 121, 381–402. (doi:10.1016/S0022-5193(86)80098-4)
- 17. Cortez R. 2001 The method of regularized Stokeslets. SIAM J. Sci. Comput. 23, 1204–1225. (doi:10.1137/S106482750038146X)
- 18. Cortez R, Fauci L, Medovikov A. 2005 The method of regularized Stokeslets in three dimensions: analysis, validation, and application to helical swimming. *Phys. Fluids* 17, 031504. (doi:10.1063/1.1830486)
- 19. Ainley J, Durkin S, Embid R, Boindala P, Cortez R. 2008 The method of images for regularized Stokeslets. J. Comput. Phys. 227, 4600–4616. (doi:10.1016/j.jcp.2008.01.032)
- 20. Hyon Y, Stocker R, Fu HC. 2012 The wiggling trajectories of bacteria. J. Fluid Mech. 705, 58–76. (doi:10.1017/jfm.2012.217)
- 21. Martindale JD, Jabbarzadeh M, Fu HC. 2016 Choice of computational method for swimming and pumping with nonslender helical filaments at low Reynolds number. *Phys. Fluids* **28**, 021901. (doi:10.1063/1.4940904)
- 22. Constantino MA, Jabbarzadeh M, Fu HC, Bansil R. 2016 Helical and rod-shaped bacteria swim in helical trajectories with little additional propulsion from helical shape. Sci. Adv. 2, e1601661. (doi:10.1126/sciadv.1601661)
- 23. Pepper RE, Roper M, Ryu S, Matsumoto N, Nagai M, Stone HA. 2013 A new angle on microscopic suspension feeders near boundaries. *Biophys. J.* **105**, 1796–1804. (doi:10.1016/j. bpj.2013.08.029)
- 24. Pepper RE, Riley EE, Baron M, Hurot T, Nielsen LT, Koehl MAR, Kiørboe T, Andersen A. 2021 The effect of external flow on the feeding currents of sessile microorganisms. *J. R. Soc. Interface* **18**, 20200953. (doi:10.1098/rsif.2020.0953)
- 25. Samsami K. 2024 Data for the paper "Incorporating recirculation effects into metrics of feeding performance for current-feeding zooplankton" [Data set]. In Royal Society Interfaces. Zenodo. (doi:10.5281/zenodo.10601122)
- 26. Samsami K, Sanchez Arias L, Redd H, Stoll JR, Pepper RE, Fu HC. 2024 Incorporating recirculation effects into metrics of feeding performance for current-feeding zooplankton. Figshare. (doi:10.6084/m9.figshare.c.7090068)
- 27. Allen RD. 1973 Structures linking the myonemes, endoplasmic reticulum, and surface membranes in the contractile ciliate *Vorticella*. *J. Cell Biol.* **56**, 559–579. (doi:10.1083/jcb.56. 2.559)
- 28. Richard Allen's Image Collection—Chapter 19: Vorticella. See https://www6.pbrc.hawaii.edu/allen/ch19/.